Combined CASSCF and MR-CI Study on Photoinduced Dissociation and Isomerization of Acryloyl Chloride

Gang-Long Cui, Qian-Song Li, Feng Zhang, Wei-Hai Fang,* and Jian-Guo Yu*

Department of Chemistry, Beijing Normal University, Beijing 100875, People's Republic of China

Received: June 4, 2006; In Final Form: August 24, 2006

The potential energy surfaces of isomerization and dissociation reactions for $CH_2CHCOCl$ in the S_0, T_1, T_2, and S_1 states have been mapped with DFT, CASSCF, MP2, and MR-CI calculations. Rate constants for adiabatic and nonadiabatic processes have been calculated with the RRKM rate theory, in conjugation with the vibronic interaction method. Mechanistic photochemistry of $CH_2CHCOCl$ at 230−310 nm has been characterized through the computed potential energy surfaces and rate constants. Upon photoexcitation of $CH_2CHCOCl$ at 310 nm, the $S_1 \rightarrow T_1$ intersystem crossing is the dominant primary process, which is followed by the 1,3-Cl migration along the T_1 pathway. Meanwhile, the $S_1 \rightarrow S_0$ internal conversion occurs with considerable probability and the subsequent trans−cis isomerization proceeds in the ground state. The C−Cl bond cleavage is an exclusive primary channel upon photoexcitation of gaseous $CH_2CHCOCl$ at 230 nm. The direct C−Cl bond cleavage is partially blocked by effects of the matrix, and the internal conversion from S_1 to S_0 becomes an important process for the excited molecule to deactivate in the condensed phase. The present calculations not only provide a reasonable explanation of the experimental findings, but also give new insight into the mechanistic photochemistry of $CH_2CHCOCl$.

1. Introduction

The α,*β*-unsaturated carbonyl compounds constitute interesting building blocks for further functionalization by various reactions in organic chemistry and have many important applications in the medical and biological fields.[1,2] They can undergo photoinduced cycloadditions and ring closure of the C═C−C═O moiety in the acyclic compounds. These reactions have been the subject of numerous experimental and theoretical investigations.[3−14] In addition to the cycloaddition and ring closure reactions, photodissociation (fission of a bond α to the carbonyl group) and photochemical (1,*n*) sigmatropic rearrangements have been experimentally observed for the α,*β*-unsaturated carbonyl compounds.[5,15−19] In comparison, these reactions have received less attention from the viewpoint of theory.[20−22]

Acryloyl chloride ($CH_2CHCOCl$) serves as a simple α,*β*-unsaturated carbonyl compound, and several experiments have been done in order to elucidate its structure and reactivity.[23−26] The bond parameters of acryloyl chloride (propenoyl chloride) in the ground state have been determined by gas-phase electron diffraction at different temperature and by infrared and Raman spectra in early studies. Two distinct conformers were identified: a more stable planar s-trans form and a less stable s-cis form. The energy difference between the s-trans and s-cis forms was inferred to be less than 1.0 kcal·mol^{-1}, and the barrier to the cis−trans isomerization was estimated to be about 3.5 kcal·mol^{-1}. The thermal decomposition of acryloyl chloride has been investigated using infrared laser-powered homogeneous pyrolysis,[27] together with product analysis using gas chromatography/mass spectrometry, matrix isolation spectroscopy, and tunable diode laser spectroscopy. Decomposition is initiated by 1,2-HCl elimination, followed by further decomposition of ketene product.

Emission spectroscopy of acryloyl chloride has been studied, and the excited state reached by 199 nm was determined as mixed C═C/C═O π character.[17] It was suggested that photodissociation of $CH_2CHCOCl$ does not proceed through a single direct dissociation mechanism and that the excitation is initially to a predissociative state from which the dissociation channels are made possible. Photolysis of $CH_2CHCOCl$ at $\lambda \geq 310$ nm and $\lambda \geq 230$ nm has been carried out in argon matrix at 10 K.[15] At $\lambda \geq 310$ nm, cis−trans isomerization and isomerization to 3-chloro-1,2-propenone ($ClH_2C-CH═C═O$) were observed to be the only pathways. However, irradiation of $CH_2CHCOCl$ at $\lambda \geq 230$ nm speeds up the isomerization processes and induces the dissociation of the $CH_2Cl-CH═C═O$ intermediate via two different pathways. The first was loss of CO to form 2-chloroethylidene (ClH_2C-CH), which isomerized to vinyl chloride; the second was HCl elimination forming HCl and propadienone ($H_2C═C═C═O$), which underwent further dissociation and isomerization to produce HCCH, CO, and HCl as the final products.[15] These processes are summarized in Scheme 1.

SCHEME 1

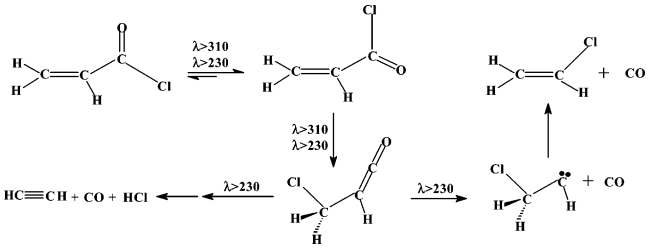

Fourier transform infrared spectra of 3-chloropropanoyl chloride (CH_2ClCH_2COCl), both as a neat liquid and isolated in an argon matrix at 10 K, have been analyzed.[16] Irradiation of CH_2ClCH_2COCl at $\lambda \geq 230$ nm yields 3-chloro-l,2-propenone and acryloyl chloride as primary photoproducts. It was found that another photon is absorbed by acryloyl chloride, giving CO, HCl, and HCCH as the final products. Photofragment translational spectroscopy was used to investigate the primary and secondary dissociation channels of the gaseous acryloyl chloride excited at 193 nm.[18] Based on the calculated heats of reactions,

10.1021/jp063457p CCC: $33.50
Published on Web 10/04/2006

four possible channels at this excitation wavelength were suggested as follows:

$$CH_2{=}CHCOCl + h\nu \rightarrow CH_2{=}CHCO + Cl \quad (1)$$

$$\rightarrow CH_2{=}CCO + HCl \quad (2)$$

$$\rightarrow CH_2{=}CH + COCl \quad (3)$$

$$\rightarrow CH_2{=}CHCl + CO \quad (4)$$

Two primary channels were observed for the C−Cl fission: one producing fragments with high kinetic recoil energies and the other producing fragments with low translational energies.[18] The high-translational-energy channel was inferred to arise from an electronic predissociation via a state repulsive in the C−Cl bond. The low-translational-energy channel was suggested to result from the C−Cl fission following internal conversion to the ground state. Another primary channel was found to be HCl elimination with the nascent CH_2CCO as a coproduct. To probe the barrier for the CH_2CHCO dissociation to $CH_2CH + CO$, photodissociation of $CH_2CHCOCl$ at 235 nm was used to produce propenoyl radicals with internal energies ranging from below to above the barrier energy of the dissociation.[19]

Complementary to the experiments, ab initio calculations have been performed in recent experimental studies.[15−19] However, these calculations focused on structures of $CH_2CHCOCl$ in the ground state, except for a CIS (configuration interaction with single excitation) calculation on the excited-state properties.[17] We have carried out ab initio calculations on photoinduced dissociation and isomerization of acrolein (CH_2CHCHO)[20] and acrylic acid ($CH_2CHCOOH$).[21,22] As a series of work devoted to photochemistry of α,β-unsaturated carbonyl compounds, the detailed mechanisms of photoinduced dissociation and isomerization for $CH_2CHCOCl$ are investigated in the present work. The potential energy surfaces of the $CH_2CHCOCl$ reactions on the ground and excited states have been characterized with the combined complete active space self-consistent field (CASSCF) and multireference configuration interaction (MR-CI) methods. The surface intersections have been determined with the state-averaged CASSCF technique. Rate constants of internal conversion (IC), intersystem crossing (ISC), and direct dissociation processes have been calculated with adiabatic and nonadiabatic rate theories. It was found that the photochemical reactivity of $CH_2CHCOCl$ is different from that of CH_2CHCHO or $CH_2CHCOOH$. We believe that the present study provides new insights into the mechanistic photochemistry of acryloyl chloride and related α,β-unsaturated carbonyl compounds.

2. Computational Methods

Ab initio molecular orbital methods have been used to investigate the ground- and excited-state potential energy surfaces (PESs) of acryloyl chloride. The stationary points on the ground-state PES are fully optimized with the MP2, B3LYP, and CASSCF energy gradient techniques. The CASSCF gradient technique is used to optimize the stationary points on the potential energy surfaces of excited singlet and triplet states. The points of surface crossing among the relevant states were determined by the state-averaged CASSCF calculations. For comparison, the B3LYP and MP2 methods were used to optimize the stationary points on the triplet surfaces. The cc-pVDZ basis set was used for all ab initio calculations. All optimization is terminated when the maximum force and its root mean square (RMS) are less than 0.00045 hartree/bohr (0.54 kcal·mol^{-1}·Å^{-1}) and 0.0003 hartree/ bohr (0.36 kcal·mol^{-1}·Å^{-1}), respectively. The nature of critical points was confirmed by an analytical frequency computation.

The choice of active space for the CASSCF computations requires some comments. To describe equilibrium structures of acryloyl chloride in low-lying electronic states, one needs the π^* and π orbitals of the C=C and C=O fragments and the n orbital located at the O atom, that is, six electrons in five orbitals. For investigating the dissociation processes that involve a breakage of the C−C or C−Cl σ bond, the C−C or C−Cl σ and σ^* orbitals should be included in the active space. This leads to an active space with eight electrons in seven orbitals, referred to as CAS(8,7), for each of the dissociation processes. The CASSCF method can give a balanced representation of the ground and excited states computed in this work. Thus, the surface topology (minima, transition states, and crossings) should be quite reliable. However, the detailed energetics will be sensitive to the inclusion of dynamic correlation. The multireference configuration interaction (MR-CI) approach is a very efficient algorithm for treating dynamic correlation, but it is a difficult task, at present, to optimize stationary structures at the MR-CI level for acrylolyl chloride. Therefore, single point energies were calculated with the MR-CI approach on the CASSCF optimized structures for the stationary points. All ab initio calculations described here had been performed with the Gaussian 03 and MOLPRO 02 program packages.[28,29]

On the basis of the calculated relative energies and frequencies for the stationary structures, as well as the energy gradients and spin−orbit coupling matrix elements at the intersection structures, rate constants for the adiabatic and nonadiabatic unimolecular processes are calculated with the RRKM theory of rate. The rate constant of the adiabatic unimolecular reaction can be expressed as[30,31]

$$k(E) = \frac{1}{h}\frac{E}{s}\frac{\sum_n h(E - \epsilon_n^{\ddagger})}{\sum_n h(E - \epsilon_n)}$$

where E is the total energy of an isolated molecule, $\epsilon_n^{\ddagger}$ and ϵ_n are respectively the vibrational energy levels of the transition state and the reactant molecule, and $h(x)$ is the usual step function:

$$h = \begin{cases} 0, & x < 0 \\ 1, & x > 0 \end{cases}$$

A simple way to include the nonadiabatic effect is to consider it as a factor of transition probability, just like Miller dealing with the tunneling effect.[32] The expression for the nonadiabatic unimolecular rate constant is in the form of

$$k(E) = \frac{1}{h}\frac{E}{s}\frac{\sum_n P(E - \epsilon_n^{\ddagger})}{\sum_n h(E - \epsilon_n)}$$

The hopping probability P is calculated with the expression developed by Delos:[33]

$$P_{\mathrm{Delos}}(E - \epsilon_n) = 4\pi^2 V_{12}{}^2 \left(\frac{2\mu_h}{\hbar^2 F \Delta F}\right)^{2/3} A_i{}^2 \left[(E - \epsilon_n)\left(\frac{2\mu_h \Delta F^2}{\hbar^2 F^4}\right)^{1/3}\right]$$

where V_{12} is the spin−orbit coupling matrix element that couples the singlet and triplet surfaces, μ_h is the effective reduced mass, ΔF is the norm of difference of the gradients on the two crossing surface, $|\partial V_1/\partial q - \partial V_2/\partial q|$, and F is the geometric mean of the norms of the two gradients, $\sqrt{|\partial V_1/\partial q| \times |\partial V_2/\partial q|}$.

A general expression for calculation of the internal conversion rate constant has been developed by Lin and co-workers.[34] The rate constant is given by

$$W_{if} = \sum_l \frac{1}{\hbar^2}\left(\frac{\varpi_l}{2\hbar}\left|R_l(fi)\right|^2\right)\sqrt{\frac{2\pi}{\sum_j S_j \varpi_j^2(2\bar{n}_j+1)}}\exp\left(-\frac{(\varpi_{fi}+\varpi_l+\sum_j S_j\varpi_j)^2}{2\sum_j S_j\varpi_j^2(2\bar{n}_j+1)}\right)$$

where "i" and "f" mean the initial and final states, respectively; R_l(fi) represents the coupling between the electronic wave functions of the two states:

$$R_l(\mathrm{fi}) = -\hbar^2\langle\Phi_f|\partial/\partial Q_l|\Phi_i\rangle$$

ϖ_{fi} is the energy difference between the initial and final states; S_j is the Huang−Rhys factor for the jth mode:

$$S_j = (\omega_j/2\hbar)\Delta Q_j^2$$

ΔQ_j is the displacement of the oscillator from the initial to final state for the jth mode, which is calculated as $\Delta Q = |L|\cdot\Delta q$. $\bar{n}_j = kT/\hbar\varpi$ is the thermally averaged number of phonons for the jth mode in the Boltzmann distribution.

3. Results and Discussion

A. S_0, T_1, T_2, and S_1 Structures. Geometric and electronic structures are basic, but important, properties of a molecule. However, there is a general lack of information on the structures and properties of acryloyl chloride in the excited electronic states. Before discussing the dissociation and isomerization pathways, we pay a little attention to the electronic and geometric structures of $CH_2CHCOCl$ in the low-lying electronic states. Acyloyl chloride exists in s-trans and s-cis forms with respect to the C−C single bond. The CAS(8,7), MP2, and B3LYP calculations predict that s-trans and s-cis equilibrium geometries in the ground state have the C_s symmetry, which is consistent with the experimental findings.[26] Because of the conjugation interaction between the C═C and C═O double bonds, the intermediate C−C bond is partially of double bond character. The experimental C−C, C−H, and C═O bond lengths are well reproduced by the CAS(8,7), B3LYP, and MP2 calculations. However, there exists considerable difference in theoretical and experimental C−Cl bond lengths. The C−Cl bond length in the s-trans form is 1.836, 1.835, and 1.811 Å at the CAS(8,7), B3LYP, and MP2 levels, respectively, which was inferred to be 1.804 Å by gas-phase electron diffraction[26] and 1.816 Å by microwave spectroscopy.[35] In addition, the C−Cl bond length in the s-trans form was experimentally estimated to be quite different from that in the s-cis structure.[26] However, the calculated results show that the C−Cl bond length in the s-trans form is nearly equal to that in the s-cis structure. Ab initio calculations at different levels have been performed to determine s-trans and s-cis structures of $CHClCHCOCl$ and CH_2CCH_3COBr.[36,37] The C−Cl and C−Br bond lengths in s-cis structures were predicted to be almost equal to the corresponding values in s-trans structures. The optimized structures of $CH_2CHCOCl$ are shown in Figure 1, along with the atomic numbering and the selected bond lengths. The detailed structural parameters are given in the Supporting Information.

Molecular orbital calculations predict that the lowest triplet state (T_1) originates from the C═C $\pi\rightarrow\pi^*$ excitation. Thus, this state is assigned as $^3\pi\pi^*$ hereafter. As a result of the C═C $\pi\rightarrow\pi^*$ excitation, the C1−C2 bond length is increased from 1.322 Å in the S_0 structure of the s-trans form (*trans*-S_0) to 1.466 Å in the corresponding $T_1(^3\pi\pi^*)$ state and is mainly of single bond nature. Thus, the terminal CH_2 group in the T_1 state can rotate more freely around the C1−C2 bond. The H7−C1−C2−C3 and H6−C1−C2−C3 dihedral angles are respectively −82.5° and 82.5° in the s-trans structure of the T_1 state (*trans*-T_1). The *trans*-T_1 structure has C_s symmetry with all atoms in the symmetry plane, except for the H6 and H7 atoms that lie above and below the symmetry plane, respectively. After the C═C $\pi\rightarrow\pi^*$ excitation, a new conjugation system is formed in the T_1 state, which is composed of the C═O π and p_z orbitals of Cl5 and C2 atoms. The C2−C3 and C−Cl5 bond lengths become shorter and the C═O bond length becomes longer, due to such conjugation interaction in the *trans*-T_1 structure.

The optimized geometries for the T_2 and S_1 states are shown in Figure 1. The T_2 minimum is similar to the S_1 minimum in structure. Molecular orbital calculations predict that both the S_1 and T_2 states originate from the C═O $n\rightarrow\pi^*$ excitation, and the S_1 and T_2 states are assigned as $^{1,3}n\pi^*$ hereafter. The electronic rearrangements induced by excitation from the ground state to the excited states significantly influence the structures of acryloyl chloride. It is known that the C═O $n\rightarrow\pi^*$ electron excitation results in pyramidal equilibrium structures for the $^{1,3}n\pi^*$ states of one-carbonyl compounds, such as CH_3COCH_3 and H_2CO.[38−40] However, the S_1 and T_2 states have planar structures for $CH_2CHCOCl$. The conjugation interaction between the C═C π electrons and p electrons distributed on the Cl5 and C3 atoms makes a planar structure more stable. In comparison with the S_0 structure, the largest change in the S_1 or T_2 equilibrium structure is associated with the heavy atom backbone. For example, the C3−O4 bond length is 1.348 Å in the S_1 state, 0.157 Å longer than that of 1.191 Å in the S_0 state. The Cl5−C3 and C3−C2 distances are decreased by 0.11 and 0.097 Å from S_0 to S_1, while the C1−C2 distance is increased by 0.086 Å in the S_1 state with respect to that in the S_0 state. Relative to the S_0 structure, the single/double bond character is almost interchanged in the S_1 and T_2 states. On the basis of the structural parameters from microwave spectroscopy and electron diffraction measurements, the excited-state molecular orbitals of *s-trans*-$CH_2CHCOCl$ were calculated with the CIS method.[17] The CIS calculations revealed that the antibonding has mixed π^*(C═C)/π^*(C═O) character, which is consistent with that reported here. However, the excited state was identified as the $^1\pi\pi^*$ state, which is different from the present identification of $^1n\pi^*$ as the first excited singlet state.

B. Relative Energies of the T_1, T_2, and S_1 States. The relative energy of the T_1, T_2, or S_1 state is determined as the energy difference between the S_0 state and the T_1, T_2, or S_1 state of *s-trans*-$CH_2CHCOCl$. The 0−0 energy gap between S_0 and T_1 is predicted to be 55.0, 65.3, and 66.8 kcal·mol^{-1} by the B3LYP, CAS(8,7), and MP2 calculations, respectively. On the basis of the CAS(8,7) optimized S_0 and T_1 structures, the relative energy of the T_1 state is calculated to be 60.0 kcal·mol^{-1}

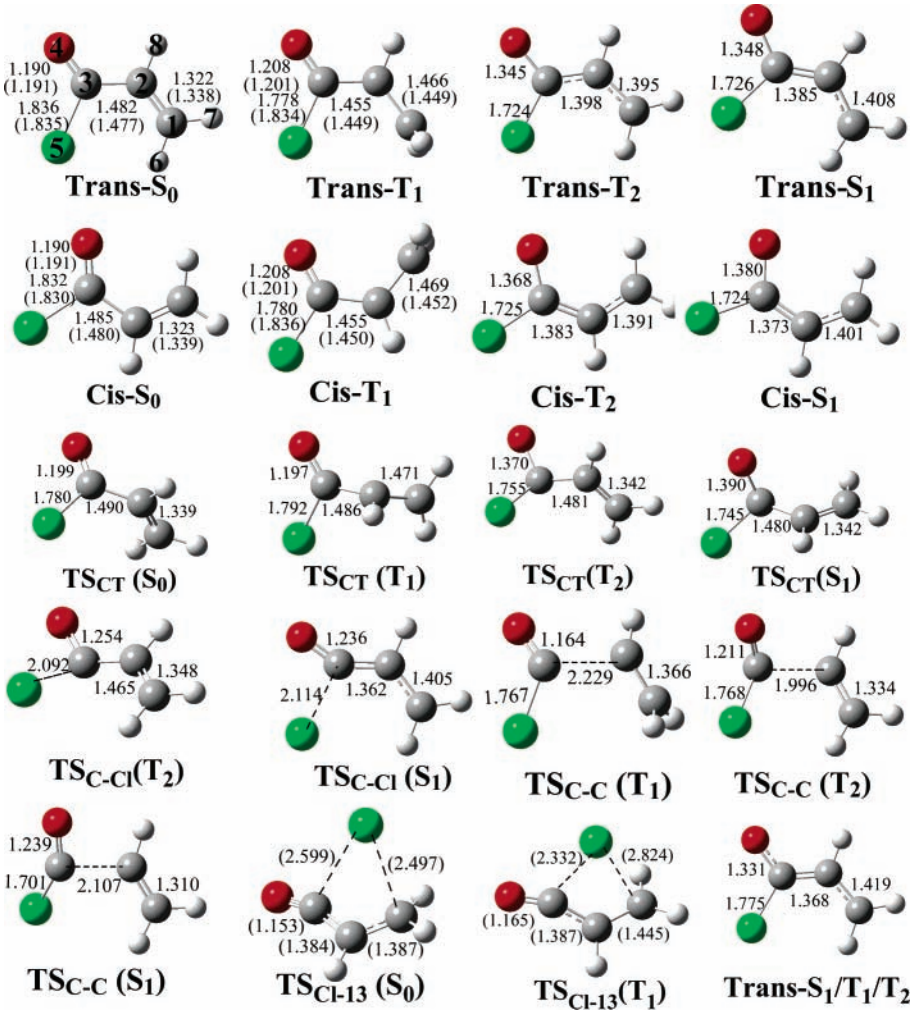

Figure 1. Stationary and intersection structures on the S_0, S_1, T_1, and T_2 potential energy surfaces of $CH_2CHCOCl$, along with the key bond lengths (Å) from the CAS(8,7) and B3LYP (in parentheses) calculations.

by the MR-CI single energy calculations with the CAS(8,7) vibrational zero point energy correction. Generally, the T_1 relative energy is a little underestimated and overestimated by the B3LYP and MP2 methods, respectively. The MR-CI calculations provide the best description of the relative energy of the T_1 state. The adiabatic excitation energies to T_2 and S_1 are predicted to be respectively 93.5 and 95.8 kcal·mol^{-1} at the CAS(8,7) level. They become 91.3 and 96.9 kcal·mol^{-1}, respectively, by the MR-CI calculations with the CAS(8,7) vibrational zero point energy correction. No experimental data are available in the literature on the $S_0 \rightarrow T_2$ or $S_0 \rightarrow S_1$ band origin for $CH_2CHCOCl$. The relative energy of the S_1 state was estimated at 109.3 kcal·mol^{-1} by the MP2/6-31G* calculation.[15]

C. The cis−trans Isomerization Reactions. The s-trans and s-cis isomers were identified for $CH_2CHCOCl$ in the ground state.[26] The s-cis isomer was observed as one of the initial products upon irradiation of *s-trans*-$CH_2CHCOCl$ in argon matrix at 10 K.[15] The cis−trans isomerization reaction can take place either in the ground state or in an excited state. The potential energy profiles for the cis−trans isomerization reactions in the S_0, T_1, T_2, and S_1 states have been characterized in this subsection, and the detailed mechanism will be discussed below.

Four transition states on the S_0, T_1, T_2, and S_1 isomerization pathways were found, which are referred to as $TS_{CT}(S_0)$, $TS_{CT}(T_1)$, $TS_{CT}(T_2)$, and $TS_{CT}(S_1)$, respectively. As shown in Figure 1, the cis−trans isomerization processes involve a rotation of the CH_2CH group around the C2−C3 bond. In the $TS_{CT}(S_0)$ structure, the CH_2CH and COCl groups are nearly perpendicular to each other with the C1═C2−C3═O4 dihedral angle of −97.6°. With respect to the zero point level of *trans*-S_0, the barrier to the cis−trans isomerization is 12.0 kcal·mol^{-1} at the CAS(8,7) level and 6.4 kcal·mol^{-1} at the MR-CI level. The barrier was experimentally inferred to be about 3.5 kcal·mol^{-1}.[26] The barrier to the cis−trans isomerization was predicted to be about 8.0 kcal·mol^{-1} for CH_2CCH_3COBr in the ground state.[32] The cis−trans isomerization along the T_1 pathway has a barrier of 5.8 kcal·mol^{-1} at the MR-CI level, which is close to that on the S_0 pathway. As pointed out above, the S_1 and T_2 states have planar structures for $CH_2CHCOCl$ and the C2−C3 bond is of double bond character in the S_1 and T_2 structures. It can be expected that the S_1 and T_2 cis−trans isomerization reactions take place with more difficulty than the isomerization along the S_0 pathway. The MR-CI single point energy calculations on the CAS(8,7) optimized structures give barriers of 18.9 and 16.9 kcal·mol^{-1} on the T_2 and S_1 pathways, respectively. The potential energy profiles of the cis−trans isomerization are plotted in Figure 2a along the MR-CI relative energies.

D. 1,3-Cl Migration Reaction. During the photolysis of $CH_2CHCOCl$ at $\lambda \geq 310$ nm, 3-chloro-1,2-propenone ($ClH_2C-CH=C=O$) was the only observed product,[15] which comes from the 1,3-Cl migration of $CH_2CHCOCl$. The transition state of the 1,3-Cl migration in the ground state, $TS_{Cl-13}(S_0)$, was optimized with the MP2/6-31G* method,[15] and the activation barrier was

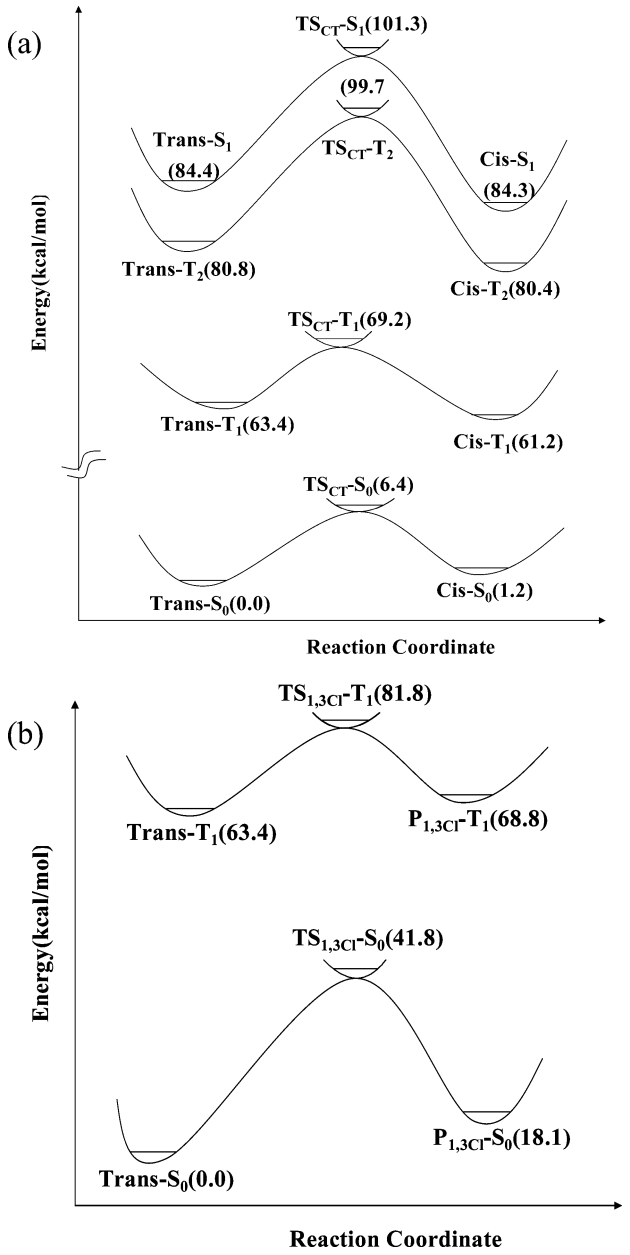

Figure 2. Schematic potential energy profiles for the cis−trans isomerization (a) and the 1,3-Cl migration (b) on the different electronic states, along the MR-CI relative energies (kcal·mol^{-1}) of stationary structures.

calculated to be 49.6 kcal·mol^{-1}. The $TS_{Cl-13}(S_0)$ structure is reoptimized with the MP2 and B3LYP methods in conjugation with the cc-pVDZ basis set, and the barrier is predicted to be 46.5 and 38.7 kcal·mol^{-1} at the MP2 and B3LYP levels, respectively. The barrier is determined to be 41.8 kcal·mol^{-1} by the MR-CI single point calculations. Considering that the MP2 calculations generally overestimate a barrier by a few kilocalories per mole and the relative energy of a transition state is underestimated by the B3LYP calculation, the MR-CI calculation provides a good estimation of the barrier for the 1,3-Cl migration in the ground state. The potential energy profiles for the 1,3-Cl migration are plotted in Figure 2b, together with the MR-CI relative energies.

As shown in Figure 1, the terminal CH_2 group rotates about 90° from the *trans*- $CH_2CHCOCl(S_0)$ to the *trans*-$CH_2CHCOCl$-(T_1) structure. The twisted *trans*-$CH_2CHCOCl(T_1)$ equilibrium geometry provides a good opportunity for the Cl5 migration from C3 to C1 atom, which gives us a hint that the 1,3-Cl migration proceeds more easily along the T_1 pathway than in the S_0 state. A transition state on the T_1 pathway, $TS_{Cl-13}(T_1)$, was found for the 1,3-Cl migration. The $TS_{Cl-13}(T_1)$ structure is shown in Figure 1 along with the selected B3LYP/cc-pVDZ bond parameters. The 1,3-Cl migration along the T_1 pathway has a barrier of 16.9 and 18.4 kcal·mol^{-1} at the B3LYP and MR-CI levels, respectively. As expected, this barrier is much lower than that on the S_0 pathway. Unlike the T_1 state, the *trans*-$CH_2CHCOCl(S_1)$ and *trans*-$CH_2CHCOCl(T_2)$ structures are planar and a coplanar migration of the Cl atom occurs with much difficulty, due to steric effects. We attempted to locate a transition state on the S_1 or T_2 pathway and found that the barrier is very high for the 1,3-Cl migration on the S_1 or T_2 pathway. Relative to the S_0 zero level, the barrier on the S_1 pathway was estimated to be 121.8 kcal·mol^{-1} by the MP2/6-31G* calculation.[15] Therefore, the 1,3-Cl migration occurs with little probability for $CH_2CHCOCl$ in the S_1 or T_2 state.

E. The C−Cl α-Cleavage Reaction. The CH_2CHCO radical in the ground state is planar with $^2A'$ symmetry. This state, together with the ground-state Cl atom (^2P), can correlate with three singlet and three triplet states of acryloyl chloride. The dissociation of $CH_2CHCOCl$ to CH_2CHCO and Cl in the ground state is endothermic by 86.8 kcal·mol^{-1} without any barrier above the endothermicity. A nonplanar transition state on the triplet pathway is found by the CAS(8,7) calculations. Based on the calculated molecular orbitals, structural parameters, and the displacement vectors associated with the imaginary vibrational mode, the transition state is deduced to connect the T_2 state of $CH_2CHCOCl$ on the reactant side. This triplet transition state is referred to as $TS_{C-Cl}(T_2)$ hereafter. The C−Cl α-bond cleavage starting from the T_2 state has a barrier of 11.7 kcal·mol^{-1} at the CAS(8,7) level and 9.5 kcal·mol^{-1} at the MR-CI level. A nonplanar transition state, $TS_{C-Cl}(S_1)$, is determined by the CAS(8,7) calculation, which is similar to $TS_{C-Cl}(T_2)$ in structure. With respect to the minimum of the S_1 state, the barrier height is 12.1 kcal·mol^{-1} at the CAS(8,7) level and 8.8 kcal·mol^{-1} at the MR-CI level. The potential energy profiles for the C−Cl α-bond cleavage are shown in Figure 3a, where the MR-CI relative energies are also given. We attempted to optimize a transition state for the C−Cl α-bond cleavage on the T_1 pathway, but the optimization always leads to the transition state of $TS_{Cl-13}(T_1)$ for the 1,3-Cl migration on the T_1 state.

F. The C−C α-Cleavage Reaction. The C−C α-bond cleavage of $CH_2CHCOCl$ leads to formation of the CH_2CH and COCl radicals. When the two radicals in the ground state approach each other, they can correlate adiabatically with a triplet state of acryloyl chloride, besides correlating with the ground state. The potential energy profile of the C−C α-bond cleavage is scanned from the S_0 equilibrium bond length to the dissociation limit of $CH_2CH(^2A')$ and $COCl(^2A')$. The C−C α-bond cleavage in the ground state is found to be endothermic by 76.9 kcal·mol^{-1} with no potential barrier above the endothermic character.

The lowest triplet surface of acryloyl chloride along the pathway of nuclear geometries that leads to CH_2CH and COCl can be viewed as originating from the interaction of an excited $^3\pi\pi^*$ configuration and a locally excited $^3\sigma\sigma^*$ configuration of the C2−C3 bond. The former is lower in energy at the initial geometry, as the latter is at the final geometries. Somewhere along the way they tend toward crossing, but the cross is avoided and results in a barrier separating the two minima on the lowest triplet surface. A transition state, $TS_{C-C}(T_1)$, is confirmed on the T_1 pathway to $CH_2CH(^2A')$ and $COCl(^2A')$ by the CAS-

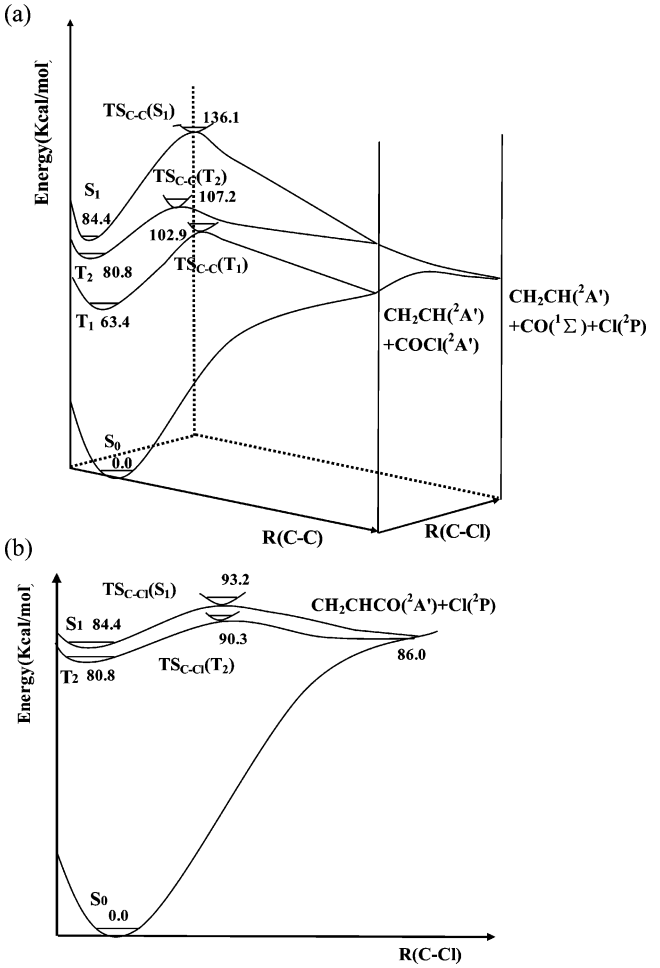

Figure 3. Schematic potential energy profiles for the C−Cl (a) and C−C (b) bond cleavages on the different electronic states, along the MR-CI relative energies (kcal·mol^{-1}) of stationary structures.

(8,7) calculations. With respect to the S_0 zero level, the $TS_{C-C}(T_1)$ transition state has relative energies of 116.2 and 102.9 kcal·mol^{-1} at the CAS(8,7) and MR-CI levels, respectively.

As shown in Figure 1, the CH_2CH and COCl moieties are nearly perpendicular to each other in the $TS_{C-C}(T_1)$ structure, which is required by a structural feature of the T_1 state. Another transition state on the triplet pathway is found, where the CH_2-CH moiety is almost coplanar with the COCl group. This transition state, referred to as $TS_{C-C}(T_2)$ hereafter, is confirmed to connect the T_2 state of $CH_2CHCOCl$ on the reactant side. With respect to the S_0 zero level, the $TS_{C-C}(T_2)$ transition state has relative energies of 126.3 and 107.2 kcal·mol^{-1} at the CAS-(8,7) and MR-CI levels, respectively. Using the $TS_{C-C}(T_2)$ geometry and molecular orbital as the initial guess, the transition state for the α-C−C bond fission on the S_1 state is optimized with the CAS(8,7) method. The optimized structure, denoted by $TS_{C-C}(S_1)$, is shown in Figure 1. From the displacement vectors associated with the imaginary vibration mode of $TS_{C-C}(S_1)$, it can be deduced that $TS_{C-C}(S_1)$ is the transition state connecting the *trans*-S_1 reactant and excited-state products (Figure 2). Relative to the S_0 state, the barrier is calculated to be 136.1 kcal·mol^{-1} at the MR-CI level with the CAS(8,7) zero point correction. Qualitatively, the C−C bond cleavage of CH_2-CHCOCl along the S_1 or T_2 pathway yields the fragment of COCl in the excited electronic state ($^2A''$). However, the COCl radical in the $^2A''$ state is unstable and dissociates into CO + Cl immediately after the C−C bond fission. Thus, the S_1 or T_2 C−C bond cleavage can be considered as a three-body dissociation to CH_2═CH, CO, and Cl in the ground state. Actually, the COCl radical in the ground state decomposes easily to CO and Cl with a barrier of 3.2 kcal·mol^{-1} at the MP2/cc-pVDZ level. The potential energy profiles of the reaction are shown in Figure 3b.

TABLE 1: Rate Constants (k) as a Function of Transition Energy (kcal·mol^{-1}) for Adiabatic and Nonadiabatic Processes of the S_1 State

transition energy	$k_{C-Cl}(S_1)/s^{-1}$	$k_{ISC}(S_1 \rightarrow T_1)/s^{-1}$	$k_{IC}(S_1 \rightarrow S_0)/s^{-1}$
92.2	0.0	6.8×10^5	1.9×10^5
100.0	3.3×10^{10}	1.2×10^7	1.2×10^8
115.4	5.1×10^{12}	1.4×10^8	1.1×10^{10}
124.4	1.4×10^{13}	2.9×10^8	3.6×10^{10}

4. Mechanistic Aspects

A. The S_1, T_1, and T_2 Surface Intersections. Photoinduced isomerization and dissociation of $CH_2CHCOCl$ are probably nonadiabatic processes. Therefore, intersections of different potential energy surfaces play an important role in understanding the mechanistic photochemistry of acryloyl chloride. With the *trans*-S_1 structure as the initial guess, structure of the S_1 and T_2 surface intersection (S_1/T_2) is optimized by searching for the lowest energy point of the two surface crossing seams. Slater determinants are used in the state-average CAS(8,7) optimizations of the S_1/T_2 structure. The S_1/T_2 crossing point is similar to the *trans*-S_1 minimum in structure. With respect to the S_1 minimum, the S_1/T_2 intersection point has the energy of 2.3 kcal·mol^{-1} at the CAS(8,7) level. The T_1 and T_2 surface intersection (T_1/T_2) in the Franck−Condon (FC) region is optimized with the state-averaged CAS(8,7) approach. It is found that the T_1/T_2 and S_1/T_2 crossing points are indistinguishable in structure and the two crossing points are almost equal in energy. Actually, the S_1, T_1, and T_2 surfaces intersect at the same region, referred to as *trans*-$S_1/T_1/T_2$. The optimized *trans*-$S_1/T_1/T_2$ structure is shown in Figure 1 along with the selected CAS(8,7) bond parameters.

B. Adiabatic and Nonadiabatic Rate Constants. On the basis of the CAS(8,7) calculated vibrational frequencies and the MR-CI relative energies for the stationary structures on the S_1 surface, adiabatic RRKM theory of rate is employed to calculate the rate constants for the C−Cl single bond cleavage along the S_1 pathway. Only vibrational degrees of freedom are considered in the present calculation with a harmonic approximation. The rate constant for the C−Cl bond cleavage along the S_1 pathway is calculated as a function of the transition energy with a total angular momentum of $J = 0$. Since the tunneling effect is not considered in the RRKM rate calculation, the rate constant is equal to zero when the available energy is less than the barrier energy. The calculated results are listed in Table 1. The spin−orbit coupling matrix element at the *trans*-$S_1/T_1/T_2$ structure is calculated to be 62.0 cm^{-1} using a one-electron approximation for the spin−orbital coupling operator with the effective nuclear charges of Koseki et al.[41] This value is used as V_{12} for calculation of the $S_1 \rightarrow T_1$ hopping probability. The calculated $S_1 \rightarrow T_1$ ISC rate constants are listed in Table 1 as a function of the transition energy. Using the CAS(8,7)/cc-pVDZ calculated vibrational frequencies and normal coordinates of the S_0 and S_1 states, the MR-CI calculated adiabatic excitation energy, and the transition matrix elements of one-electron electric field operator, the $S_1 \rightarrow S_0$ IC rate constant is calculated to be 6.5×10^9 s^{-1} from the vibrational zero level of the S_1 state.

C. Mechanistic Photochemistry. Upon photoexcitation at $\lambda \geq 310$ nm ($\leq$92.2 kcal·mol^{-1}), the C−Cl α-bond fission along the S_1 pathway (with a barrier of 93.2 kcal·mol^{-1}) is nearly inaccessible in energy. In this case, the $CH_2CHCOCl$ molecules on the S_1 state can deactivate via internal conversion to the S_0 state or intersystem crossing to the T_1 state. The rate constant of the ISC process is estimated to be 6.8×10^5 s^{-1} at 310 nm, while the IC to the ground state has a rate constant of 1.9×10^5 s^{-1} at this excitation wavelength. The calculated rate constants reveal that the IC to the S_0 state can compete with the ISC to the T_1 state upon photoexcitation at 310 nm, but the ISC process has some preference over the IC process. The ISC process probably becomes a dominant route in argon matrix at 10 K due to the effect of heavy atom. As pointed out before, the 1,3-Cl migration has a barrier of 16.9 kcal·mol^{-1} on the T_1 pathway. Once in the T_1 state, the $CH_2CHCOCl$ molecules have enough internal energies to overcome the barrier to the 1,3-Cl migration, yielding 3-chloro-1,2-propenone. However, the trans−cis isomerization takes place very easily after internal conversion to the ground state, since the barrier (41.8 kcal·mol^{-1}) of the 1,3-Cl migration is much higher than that (6.4 kcal·mol^{-1}) for the isomerization on the S_0 pathway. The 1,3-Cl migration was observed to be a dominant pathway and the trans−cis isomerization plays a minor role in the photolysis of $CH_2CHCOCl$ at $\lambda \geq 310$ in argon matrix at 10 K.[15] This gives us reason to expect that the 1,3-Cl migration proceeds along the T_1 pathway as a result of the $S_1 \rightarrow T_1$ intersystem crossing.

Relative to the S_0 zero level, the C−Cl bond cleavage has a barrier of 93.2 kcal·mol^{-1} along the S_1 pathway. The ISC process is not in competition with the direct C−Cl bond cleavage upon irradiation of gaseous $CH_2CHCOCl$ at 230 nm, and the IC process could play a minor role at this excitation wavelength. These can be seen from the calculated rate constants in Table 1. The C−Cl bond cleavage was observed to be the primary dissociation channel of gaseous acryloyl chloride excited at 193 nm.[18,19] In argon matrix at 10 K, the barrier to the C−Cl bond cleavage is considerably increased due to the matrix effect.[42] As a result, the internal conversion from S_1 to S_0 becomes an important process for the excited molecule to deactivate in the matrix. In addition, the S_0 and S_1 states are degenerate at large C−Cl separation. Before the C−Cl bond is completely broken along the S_1 pathway, the $CH_2CHCOCl$ molecule can be re-formed in the matrix, which is followed by isomerization reactions in the ground state. The isomerization processes were found to be speeded up upon irradiation of $CH_2CHCOCl$ in argon matrix at $\lambda \geq 230$ nm and CO, HCl, HCCH, and CH_2CHCl were assigned as the final products.[15]

Since acrolein, acrylic acid, and acryloyl chloride belong to the CH_2CHCOX (X = H, OH, and Cl) series, we pay attention to the effect of the X substitution on structure and reactivity before the end of this section. CH_2CHCHO, $CH_2CHCOCl$, and $CH_2CHCOOH$ have similar S_0 structures, except for more isomers for $CH_2CHCOOH$ due to different orientation of the O−H group.[13,20−22] The $S_1(^1n\pi^*)$ and $T_2(^3n\pi^*)$ structures are planar for CH_2CHCHO and $CH_2CHCOCl$ with the C−C=C−O backbone structure. However, the $S_1(^1n\pi^*)$ and $T_2(^3n\pi^*)$ structures are nonplanar for $CH_2CHCOOH$ and the O−H group deviates from the molecular backbone by about 60.0°.[21] Because of the conjugation interaction, fission of the C−C bond α to the carbonyl group proceeds with great difficulty for the three molecules in the $S_1(^1n\pi^*)$ state. The C−H α-bond cleavage has a high barrier on the $S_1(^1n\pi^*)$ pathway, and the $S_1(^1n\pi^*) \rightarrow T_1(^3\pi\pi^*)$ intersystem crossing occurs very easily for CH_2CHCHO. As a result, the $S_1 \rightarrow T_1$ ISC followed by dissociation and isomerization reactions on the T_1 state is the dominant pathway upon photoexcitation of CH_2CHCHO at 193 nm.[13,21] In comparison with CH_2CHCHO, the $S_1 \rightarrow T_1$ intersystem crossing takes place with more difficulty and the C−O bond single fission proceeds more easily along the S_1 pathway for $CH_2CHCOOH$. In the irradiation of $CH_2CHCOOH$ at 248 and 193 nm, the S_1 direct C−O bond fission and the $S_1 \rightarrow T_1$ intersystem crossing are a pair of competitive routes. As pointed out above, there is a barrier of 8.8 kcal·mol^{-1} on the S_1 pathway of the C−Cl bond cleavage for $CH_2CHCOCl$. The C−Cl bond cleavage is an exclusive primary channel of gaseous acryloyl chloride excited at 230 nm and shorter wavelengths.

5. Summary

The potential energy surfaces of isomerization and dissociation reactions for $CH_2CHCOCl$ in the S_0, T_1, T_2, and S_1 states have been mapped with DFT, CASSCF, MP2, and MR-CI calculations. The T_1, T_2, and S_1 states were respectively characterized as $^3\pi\pi^*$, $^3n\pi^*$, and $^1n\pi^*$ in nature on the basis of the CASSCF wave functions and their electronic populations. The $S_1/T_2/T_1$ three-surface intersection structure is determined by the state-averaged CAS(8,7) calculations, which plays an important role in the $S_1 \rightarrow T_1$ intersystem crossing. Rate constants for the direct dissociation and the ISC process were calculated with adiabatic and nonadiabatic RRKM theory, while the IC rate was determined using the vibronic interaction method. The mechanistic photochemistry of $CH_2CHCOCl$ at 230−310 nm has been characterized through the computed potential energy surfaces, the optimized surface crossing structure, and rate calculations. Upon photoexcitation of $CH_2CHCOCl$ at 310 nm, the $S_1 \rightarrow T_1$ intersystem crossing is the dominant primary process, which is followed by the 1,3-Cl migration along the T_1 pathway. Meanwhile, the $S_1 \rightarrow S_0$ internal conversion occurs with considerable probability at this excitation wavelength and the subsequent trans−cis isomerization proceeds in the ground state. The C−Cl bond cleavage is an exclusive primary channel upon photoexcitation of gaseous $CH_2CHCOCl$ at 230 nm and shorter wavelengths. The direct C−Cl bond cleavage is partially blocked by effects of the matrix. As a result, the internal conversion from S_1 to S_0 becomes an important process for the excited molecule to deactivate in the condensed phase, which is followed by isomerization reactions in the ground state. The present calculations not only provide a reasonable explanation of the experimental findings, but also give new insight into the mechanistic photochemistry of $CH_2CHCOCl$ and related carbonyl compounds.

Acknowledgment. This work was supported by grants from the National Natural Science Foundation of China (Grants 20472011, 20233020, and 20573011) and from the Major State Basic Research Development Programs (Grants 2004CB719903 and 2002CB613406).

Supporting Information Available: Cartesian coordinates, energies at the CAS(8,7), B3LYP, and MP2 levels of theory, and vibrational zero point energy at the CAS(8,7) level for the stationary structures and transition states. This material is available free of charge via the Internet at http://pubs.acs.org.

References and Notes

(1) Wortelboer, H. M.; Usta, M.; Zanden, J. J.; Bladeren, P. J.; Rietjens, I. M. C. M.; Cnubben, N. H. P. *Biochem. Pharmacol.* **2005**, *69*, 1879−1890.
(2) Billard, T. *Chem.−Eur. J.* **2006**, *12*, 975−979.
(3) Bonneau, R. *J. Am. Chem. Soc.* **1980**, *102*, 3816−3822.

(4) Friedrich, L. E.; Schuster, G. E. *J. Am. Chem. Soc.* **1969**, *91*, 7204−7205.
(5) Friedrich, L. E.; Schuster, G. B. *J. Am. Chem. Soc.* **1972**, *94*, 1193−1199.
(6) Schuster, D. I. In *The chemistry of enones*; Patai, S., Rappoport, Z., Eds.; John Wiley and Sons: Chichester, U.K., 1989; Vol. 2, pp 693−756.
(7) Hamada, Y.; Nishimura, Y.; Tsumoi, M. *Chem. Phys.* **1985**, *100*, 365−375.
(8) Guerin, D. J.; Miller, S. J. *J. Am. Chem. Soc.* **2002**, *124*, 2134−2136.
(9) Brocksom, T. J.; Coelho, F.; Depres, J. P.; Greene, A. E.; de Lima M. E. F.; Hamelin, O.; Hartmann, B.; Kanazawa, A. M.; Wang, Y. Y. *J. Am. Chem. Soc.* **2002**, *124*, 15313−15325.
(10) Chatani, N.; Oshita, M.; Tobisu, M.; Ishii, Y.; Murai, S. *J. Am. Chem. Soc.* **2003**, *125*, 7812−7813.
(11) Oshita, M.; Yamashita, K.; Tobisu, M.; Chatani, N. *J. Am. Chem. Soc.* **2005**, *127*, 761−766.
(12) Arno, M.; Picher, M. T.; Domingo, L. R.; Andres, J. *Chem.−Eur. J.* **2004**, *10*, 4742−4749.
(13) Reguero, M.; Olivucci, M.; Bermardi, F.; Robb, M. A. *J. Am. Chem. Soc.* **1994**, *116*, 2103−2114.
(14) Wilsey, S.; González, L.; Robb, M. A.; Houk, K. N. *J. Am. Chem. Soc.* **2000**, *122*, 5866−5876.
(15) Pietri, N.; Monnier, M.; Aycard, J.-P. *J. Org. Chem.* **1998**, *63*, 2462−2468.
(16) Pietri, N.; Piot, J.; Aycard, J.-P. *J. Mol. Struct.* **1998**, *443*, 163−173.
(17) Arendt, M. F.; Browning, P. W.; Butler, L. J. *J. Chem. Phys.* **1995**, *103*, 5877−5885.
(18) Szpunar, D. E.; Miller, J. L.; Butler, L. J.; Qi, F. *J. Chem. Phys.* **2004**, *120*, 4223−4230.
(19) Lau, K. C.; Liu, Y.; Butler, L. J. *J. Chem. Phys.* **2005**, *123*, 054322.
(20) Fang, W. H. *J. Am. Chem. Soc.* **1999**, *121*, 8376−8384.
(21) Fang, W. H. *J. Am. Chem. Soc.* **2000**, *122*, 10866−10894.
(22) Fang, W. H. *Chem. Phys. Lett.* **2000**, *325*, 683−692.
(23) Katon, J. E.; Feairheller, W. R., Jr. *J. Chem. Phys.* **1967**, *47*, 1248−1255.
(24) Keirns, J. J.; Curl, R. F., Jr. *J. Chem. Phys.* **1968**, *48*, 3773−3778.
(25) Durig, J. R.; Church, J. S.; Compton, D. A. C. *J. Chem. Phys.* **1979**, *71*, 1175−1182.
(26) Hagen, K.; Hedberg, K. *J. Am. Chem. Soc.* **1984**, *106*, 6150−6155.
(27) Allen, G. R.; Russell, D. K. *New J. Chem.* **2004**, *28*, 1107−1115.
(28) Frisch, M. J.; Trucks, G. W.; Schlegel, H. B.; et al. A. *Gaussian 03*, revision A.9; Gaussian, Inc.: Pittsburgh, PA, 2003.
(29) MOLPRO is a package of ab initio programs written by H.-J. Werner, P. J. Knowles, and co-workers.
(30) Robbinson, P. J.; Holbrook, K. A. *Unimolecular Reactions*; Wiley: New York, 1972.
(31) Forst, W. *Theory of Unimolecular Reactions*; Academic Press: New York, 1973.
(32) Miller, W. H. *J. Am. Chem. Soc.* **1979**, *101*, 6810−6814.
(33) Delos, J. B.; Thorson, W. R. *Phys. Rev A* **1972**, *6*, 728−745.
(34) Lin, S. H.; Chang, C. H.; Liang, K. K.; Chang, R.; Shiu, Y. J.; Zhang, J. M.; Yang, T. S.; Hayashi, M.; Hsu, F. C. *Adv. Chem. Phys.* **2002**, *121*, 1−88.
(35) Kewley, R.; Hemphill, D. C.; Curl, R. F., Jr. *J. Mol. Spectrosc.* **1972**, *44*, 443−452.
(36) Durig, J. R.; Drew, B. R.; Reese, C. E.; Brletic, P. A. *Spectrochim. Acta* **2000**, *56A*, 2091−2106.
(37) Sharma, A.; Gupta, V. P.; Virdi, A. *Spectrochim. Acta* **2004**, *60A*, 311−320.
(38) Liu, D.; Fang, W. H.; Fu, X. Y. *Chem. Phys. Lett.* **2000**, *325*, 86−92.
(39) Diau, E. W.-G.; Kotting, C.; Solling, T. I.; Zewail, A. H. *Chem. Phys. Chem.* **2002**, *3*, 57−78.
(40) Yamaguchi, Y.; Wesolowski, S. S.; Van Huis, T. J.; Schaefer, H. F. *J. Chem. Phys.* **1998**, *108*, 5281−5288, and references therein.
(41) Koseki, S.; Schmidt, M. W.; Gordon, M. S. *J. Phys. Chem.* **1992**, *96*, 10768−10772.
(42) Chen, S. L.; Fang, W. H. *J. Phys. Chem. A* **2006**, *110*, 944−950.